Dyes and Pigments 175 (2020) 108123

Contents lists available at ScienceDirect

Dyes and Pigments

journal homepage: http://www.elsevier.com/locate/dyepig

BODIPY-core 1,7-diphenyl-substituted derivatives for photovoltaics and OLED applications

K. Ivaniuk [a], A. Pidluzhna [a], P. Stakhira [a], G.V. Baryshnikov [b,c,*], Y.P. Kovtun [d], Z. Hotra [a,e], B. F. Minaev [c], H. Ågren [b,f]

[a] Lviv Polytechnic National University, Stepan Bandera 12, 79013, Lviv, Ukraine
[b] Division of Theoretical Chemistry and Biology, School of Engineering Sciences in Chemistry, Biotechnology and Health, KTH Royal Institute of Technology, 10691, Stockholm, Sweden
[c] Department of Chemistry and Nanomaterials Science, Bohdan Khmelnytsky National University, 18031, Cherkasy, Ukraine
[d] Institute of Organic Chemistry, National Academy of Sciences of Ukraine, 5 Murmanska Str, 02094, Kyiv, Ukraine
[e] Rzeszow University of Technology, al. Powstańców Warszawy 12, 35-959, Rzeszów, Poland
[f] College of Chemistry and Chemical Engineering, Henan University, Kaifeng, Henan, 475004, PR China

A B S T R A C T

In the current study we demonstrate an application of four previously synthesized 1,7-diphenyl-substituted BODIPY species for inverted photovoltaic cells and for organic light-emitting devices (OLEDs). Depending on the type of substituents or annulation of the pyridone rings these dyes exhibit spectral properties in the full visible region up to the near-infrared wavelengths. All the studied compounds show very strong visible absorption that can be ascribed to the low lying LUMO levels making them electronically suitable as acceptors for many donor materials. The best fabricated inverted photovoltaic device based on the BODYPI-core derivatives demonstrates a power conversion efficiency equal to 1.36% which is close to previously published reports for related species. Two kinds of deep red OLEDs (doped and undoped) with narrow electroluminescence spectra (full width at half maximum up to 45 nm) have been fabricated. Maximum brightness of 3900 cd m^{-2} and an external quantum efficiency by 2.3% were achieved for the best OLED structure.

1. Introduction

Derivatives of BODIPY (IUPAC name is 4,4-difluoro-4-bora-3a,4a-diaza-s-indacene) have attracted growing attention during recent years as promising materials for organic light-emitting diodes [1–4], biosensors [3], solar energy convertors [5,6] and telecommunication technologies [1]. Generally, the luminescence of BODIPY dyes in the solid state is significantly suppressed due to the strong π-π stacking interactions between the rigid BODIPY planes, which lead to fluorescence self-quenching not only in the solid state but also in solutions at high concentration of BODIPY dyes. A further reason for the efficient fluorescence self-quenching of BODIPY dyes is the very small Stokes shift (5–20 nm) which leads to reabsorption of the emitted light. On the other hand, the BODIPY-core dyes usually possess attractive properties like excellent thermal, chemical, and photochemical stability, high molar absorption coefficients (up 10^5 M^{-1} cm^{-1} order of magnitude), comparatively high fluorescence quantum yields in dilute solutions, general insensitivity to both solvent polarity and pH of the environment, large cross-section for multiphoton excitation, lack of ionic charge, a good solubility in organic solvents [7–19]. Yet another advantage of BODIPY dyes is that it is possible to modulate their fluorescence wavelength in the whole visible region by simple chemical modifications as was, for example, demonstrated in Refs. [20–23]. In this respect BODIPY dyes seem to be good candidates for deep-red light harvesting which can be useful for organic photovoltaics. It is also known that BODIPY derivatives are characterized by a very low-lying (dark) first excited triplet state (T_1) relative to the first excited singlet state (S_1) that makes it possible to observe the triplet-triplet annihilation (TTA) phenomenon [24–26] and convert red/NIR quanta into UV–Vis light, being useful for sensing applications.

The fact that BODIPY-based dyes usually are characterized by narrow fluorescence spectra [7–23] is especially important for their implementation in the framework of red-green-blue (RGB) models for sensor technologies. In this respect, a design that widens the small Stokes shifts and decreases the π-π stacking interactions would open up perspectives for utilization of BODIPY derivatives in high-contrast OLEDs. In this work we have implemented the previously synthesized series of 1,7-diphenyl-substituted BODIPY dyes (compound **1**–**4** in

* Corresponding author. Division of Theoretical Chemistry and Biology, School of Engineering Sciences in Chemistry, Biotechnology and Health, KTH Royal Institute of Technology, 10691, Stockholm, Sweden.
E-mail address: glibar@kth.se (G.V. Baryshnikov).

https://doi.org/10.1016/j.dyepig.2019.108123
Received 2 August 2019; Received in revised form 9 December 2019; Accepted 9 December 2019
Available online 16 December 2019

Fig. 1) with different substituents in α- and β-positions of the BODIPY core and with fused one or two pyridine-2(1*H*)-one rings [20–23] into multilayered OLEDs and photovoltaic heterostructures.

The studied BODIPY derivatives are characterized by acceptable Stokes shifts (16–28 nm) and contain voluminous outer substituents that prevent reabsorption and aggregation-induced quenching. As a result, deep red OLEDs (electroluminescence maxima at 655 and 695 nm) with narrow electroluminescence spectra, maximum brightness of 3900 Cd m^{-2} and external quantum efficiency of 2.3% have been fabricated which is at the same level as the current state of the art for the series of BODIPY-based red/NIR OLEDs (EL maximum >650 nm) [4,27,28].

The photovoltaic cells fabricated in this work demonstrate a power conversion efficiency (η) in the range 0.2–1.4% meaning that the BODIPY derivatives can be used for light harvesting in the red region (absorption maxima in the 520–660 nm range for the different studied species). Our quantum-chemical calculations of electronic structure and spectra of the studied BODIPY derivatives together with comprehensive spectroscopic and electrochemical measurements support the fundamental understanding of the photophysical processes occurring at the molecular level in these BODIPY-core materials both in solution and in the solid state.

2. Experimental details

2.1. Cyclic voltammetry

Cyclic voltammetry (CV) measurements were carried out in the classic three-electrode system in 0.1 M solution of Bu_4NPF_6 (TCI 98%) in CH_2Cl_2 (Sigma-Aldrich, Chromasolv for HPLC) as a supporting electrolyte. A Pt disc was used as working electrode, a Pt spiral as a counter electrode, and a leak less Ag/AgCl (ET069, eDAQ) as a reference electrode. The potential was calibrated versus a ferrocene/ferrocenium redox couple.

Oxidation onset potentials (E_{ox} onset) and reduction onset potentials (E_{red} onset) were estimated from intersections of tangents to the background and oxidation or reduction peak, respectively. The energies of the highest occupied molecular orbital (E_{HOMO}) and of the lowest unoccupied molecular orbital LUMO (E_{LUMO}) were estimated from the equations $E_{LUMO} = -(E_{red}\ onset + 5.1)$ (eV) and $E_{HOMO} = -(E_{ox}\ onset + 5.1)$ (eV) [29]. The electrochemical band gap (E_g) was then easily estimated as $E_g = E_{LUMO} - E_{HOMO}$.

2.2. Photovoltaic cells fabrication

A powder of [6,6]-Phenyl-C_{61}-butyric acid methyl ester (PCBM), glass/ITO substrates and Al wire were purchased from Sigma-Aldrich. The regioregular poly(3-hexyltiophene) (P3HT) was purchased from Ossila labeled as P3HT M101 with the following characteristics (M_w = 65500 and M_n = 32000). Devices for the photovoltaic property investigations were fabricated with step-by-step procedure by the thermal-vacuum deposition technique. Glass/ITO substrates were washed consequently with distilled water, 2-propanol, NaOH in series and dried in air atmosphere. The principal scheme of the fabricated photovoltaic cells looks like this: ITO/PCBM(57 nm)/**1**–**4**(20 nm)/P3HT (50 nm)/MoO_3(8 nm)/Al(100 nm). The thickness of the films was controlled and determined using a profilometer (Dektak XT, Bruker). The photovoltaic characteristics of the fabricated cells were measured using the semiconductor parameter analyser HP4145A and the ABET technologies Solar simulator (for the standard AM 1.5G solar spectrum, the total available power is 982 W/m^2). The absorption spectra of the dyes **1**–**4** in the DCM solution and in the solid film were recorded on PerkinElmer Lambda 35 spectrometer. The photoluminescence spectra (PL) and corresponding quantum yields (PLQY) measured for the DCM solutions and thin films deposited on quartz plates were recorded with an Edinburgh Instruments FLS980 spectrometer using a low repetition rate mF920H Xenon Flash lamp as the excitation source at room temperature (excitation wavelength $\lambda_{ex} = \lambda_{abs}$).

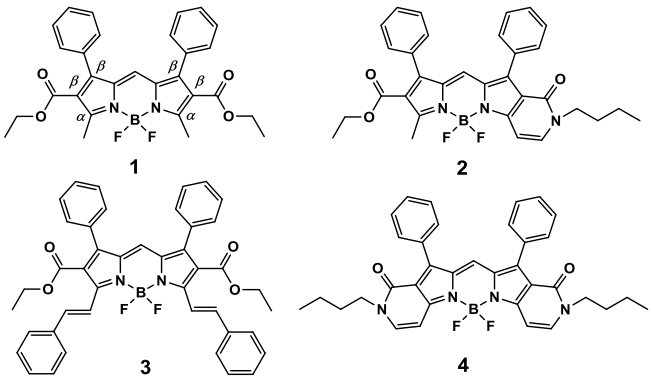

Fig. 1. BODIPY derivatives studied in the current work.

2.3. Organic light emitting diodes fabrication

The electroluminescent devices were fabricated by means of thermal vacuum evaporation of the organic compound and metal electrodes onto pre-cleaned ITO coated glass substrates with a base pressure below 10^{-5} Torr. The devices A and B were fabricated through step-by-step deposition of different organic layers and metal electrodes. CuI was used as hole-injection layer [30] and TPBi (2,2′,2"-(1,3,5-benzinetriyl)-tris (1-phenyl-1-H-benzimidazole)) and Bphen (4,7-Diphenyl-1,10-phenanthroline) – as an electron-transporting layer [31,32]. The TCTA (tris (4-carbazoyl-9-ylphenyl)amine) was implemented as a hole-transporting layer additionally [33]. The 4,4′-bis(N-carbazolyl)-1, 1′-biphenyl CBP was used as host for compounds **2** and **3** upon the fabrication of devices C and D by means thermal vacuum co-deposition [34] (dopant concentration 20%). Since Ca is highly reactive and corrodes quickly in ambient atmosphere, a Ca layer coated by 200 nm aluminium (Al) layer was used as cathode. Among the four studied compounds **1**–**4**, only materials **2** and **3** demonstrate stable electroluminescence within the OLED devices. A principal scheme of the fabricated OLEDs can be presented as follows:

A: ITO/CuI (10 nm)/TCTA (30 nm)/**2**(45 nm)/TPBi (15 nm)/Ca (30 nm)/Al (200 nm);
B: ITO/CuI (10 nm)/TCTA (30 nm)/**3**(45 nm)/TPBi (15 nm)/Ca (30 nm)/Al (200 nm);
C: ITO/CuI (10 nm)/CBP:**2** (60 nm)/Bphen (30 nm)/Ca (30 nm)/Al (200 nm);
D: ITO/CuI (10 nm)/CBP:**3** (60 nm)/Bphen (30 nm)/Ca (30 nm)/Al (200 nm).

The active area of the prepared devices was 2 × 3 mm^2. The current density-voltage and luminance-voltage dependences were recorded using the semiconductor parameter analyser HP4145A. Measurement of brightness was carried out using a calibrated photodiode. Electroluminescence (EL) spectra were recorded with the Ocean Optics USB2000 spectrometer.

3. Computational details

The structures of the BODIPY-core derivatives **1**–**4** were optimized at the B3LYP/6-31G(d) [35–37] level of density functional theory (DFT). With the same method the normal frequencies were calculated by the gradient approach to determine the true minimum of the total energy. All the vibrational mode frequencies were found to be real, which indicates true energy minimum locations. The frontier molecular orbitals (MOs) were mapped from single point energy calculations (iso-density surface values were fixed at 0.03 a.u.). The electronic excited state

properties for the studied molecules (vertical absorption and fluorescence spectra) were calculated by the time-dependent (TD) DFT method [38] using the same B3LYP functional and 6-31G(d) basis set. The solvent effect on the electronic excited states energies was taken into account using the polarized-continuum model (PCM) [39] with the dichloromethane (DCM, $\varepsilon = 2.37$) as a model solvent. All the calculations were carried out using the Gaussian 16 software [40].

4. Results and discussion

4.1. Electrochemical properties

Electrochemical measurements of compounds **1**–**4** were performed in order to accurately estimate the energies of their HOMO and LUMO levels required for the correct choice of supporting materials upon fabrication of the OLEDs and OPV cells. The final results are summarized in Table 1. One can see from this table that the theoretically estimated energies of HOMO and LUMO levels correlate well with the experimental CV measurements. Typically, calculated HOMO energies agree well with the experimental values (deviation is within 0.4 eV), while the computed LUMO energies (and thus E_g values) are significantly overestimated relative to the CV data which is a known limitation of the DFT approximation in respect to the unoccupied molecular orbitals [29,41]. The shapes of the frontier molecular orbitals are presented in Fig. 2. Both HOMO and LUMO wave functions are of π-symmetry (relative to the BODIPY core plane). One important observation is that the bonding-antibonding character for particular chemical bonds inside the BODIPY chromophore core does not change moving from HOMO to LUMO. It means that upon the electronic transition of HOMO-LUMO configuration the structure of the excited state molecules **1**–**4** should not change considerably. It also means that potential energy surfaces for the ground and excited electronic state of the HOMO-LUMO configuration are only a little shifted which is in line with the small experimentally observed Stokes shift between the 0-0 absorption and fluorescence maxima.

Fig. 3a represents the cyclic voltammograms (CVs) recorded during reduction of the studied compounds. All CVs for compounds **1**–**4** reveal quasi-reversible reduction peaks. The shift of reduction potential is observed in the series of compounds. Particularly, compound **4** undergoes reduction at the potential $E_{red\ onset}$ of 0.67 V which corresponds to E_{LUMO} of 4.21 eV implying a strong electron-acceptor character for compound **4**. It is the result of the presence of two amide groups which are known to be electron-deficient groups [41]. The $E_{red\ onset}$ potential and corresponding E_{LUMO} value for compound **2** are located between those for compounds **1** and **3** which is due to the presence of only one amide group. Similar values of $E_{red\ onset}$ and E_{LUMO} were recorded for compound **3**. The shift of $E_{red\ onset}$ from compound **3** to compound **1** is related to the presence of additional phenylenevinylene groups which effectively increase conjugation owning to the resonance effect [41].

Fig. 3b represents CVs recorded during oxidation of the studied compounds **1**–**4**. The oxidation of the studied compounds was observed to be irreversible. Such behaviour is very similar to some other reported BODIPY-based compounds [42]. The incorporation of amide groups shifts $E_{ox\ onset}$ to lower potentials relative to the compound **1**. The similar effect was observed for compound **3** due to the effect of phenylenevinylene groups.

The analysis of the electrochemical results indicates that incorporation of amide groups as well as phenylenevinylene groups has a strong influence on the electronic properties of the BODIPY derivatives due to inductive and mesomeric effects. Actually, inclusion of amide and phenylenevinylene into the initial BODIPY derivative **1** leads to LUMO stabilization (E_{LUMO} decreases) and HOMO destabilization (E_{HOMO} increases) which finally leads to energy band gap narrowing.

Table 1
Electrochemical properties of compounds **1**–**4** measured by CV method in comparison with the quantum-chemical calculations results (in parentheses).

Compound	$E_{ox\ onset}$, V	$E_{red\ onset}$, V	E_{HOMO}, eV	E_{LUMO}, eV	E_g, eV
1	1.06	−1.14	−6.16 (−5.95)	−3.96 (−3.01)	2.20 (2.94)
2	0.81	−1.01	−5.91 (−5.58)	−4.09 (−3.10)	1.82 (2.48)
3	0.71	−1.01	−5.81 (−5.38)	−4.09 (−3.13)	1.72 (2.26)
4	0.67	−0.89	−5.77 (−5.37)	−4.21 (−3.19)	1.56 (2.18)

4.2. Photovoltaic cells performance

Considering that the studied BODIPY-core derivatives exhibit a strong absorption in the visible region (>500 nm) (Fig. 4a) and variable redox chemistry, we conceived the usage of these compounds as light harvesting materials in photovoltaic heterostructures. Actually, compounds **1**–**4** demonstrate low lying LUMO levels (Table 1), making them electronically suitable as acceptors for many electron-donor materials in bulk heterojunction solar cells [43,44]. In the current study the P3HT material was used as the donor material [45,46]. This material also plays the hole-transporting layer (HTL) function after the exciton dissociation [43].

The PCBM material was used as an electron transport layer (ETL). Together with the ETL function the PCBM material shows itself additional light harvesting in the region 300–550 nm [47]. The best OPV cell based on compound 2 demonstrates an overall performance (η) about 1.36% (Table 2) that is comparable with similar devices based on BODIPY dyes and related acceptor species [5,43,48,49]. The main photovoltaic parameters for the fabricated solar cells are also presented in Table 2, where J_{sc} is the short circuit current density, V_{oc} is the open circuit voltage, and I_{max} and V_{max} are current and voltage at maximum power point P_{max}, FF is the fill factor and η is the power conversion efficiency.

One can see from Fig. 4b that the absorption spectrum of compound **1** is significantly blue-shifted comparing to the absorption spectrum measured for diluted DCM solutions (Fig. 4a). It is caused by the strong H-aggregation of compound **1** due to the formation of plane-to-plane stacking dimers [50–52]. Inclusion of the 1-butylpyridine-2(1H)-one groups and phenylenevinylene groups (in α-positions of compound **3**) prevents aggregation in the solid state and the corresponding absorption spectra for compounds **2**–**4** are similar (just slightly broadened) to that measured in DCM solutions. The performance of the OPV cells gradually decreases in the row **2**>**3**>**4** (Table 2) which is caused by the increase of the barrier for electron injection at the interface with PCBM, respectively (LUMO level of PCBM lies at −3.7 eV, [47]).

The standalone compound **1** demonstrates the best consistence of HOMO and LUMO levels with the P3HT and PCBM adjacent layers (Table 1), but with the absence of a tandem coabsorption effect with the PCBM material the light harvesting becomes insufficient in the yellow-red region of the visible spectrum and thus the overall performance of the OPV cell becomes quite small (0.6%, Table 2).

4.3. Computational insight into the photophysics of BODIPY derivatives

In order to investigate the photophysical behaviour of the studied BODIPY-core derivatives **1**–**4,** quantum-chemical TD DFT calculations of the vertical absorption and fluorescence spectra have been performed. As can be seen form Table 3 all the studied compounds demonstrate high intensities for both $S_0 \rightarrow S_1$ and $S_1 \rightarrow S_0$ vertical electronic transitions in excellent agreement with the high molar absorption coefficients and fluorescence quantum yields observed experimentally.

The small differences between the vertical and adiabatic energies of fluorescent $S_1 \rightarrow S_0$ transitions (20–30 nm) imply that the shift of the S_1 excited state potential energy hypersurface relative to the ground

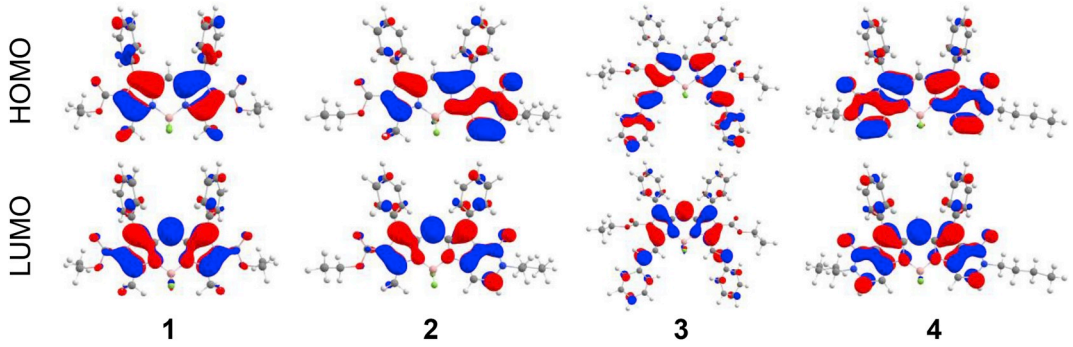

Fig. 2. The shape of frontier molecular orbitals of the compounds **1**–**4** calculated by the B3LYP/6-31G(d) method.

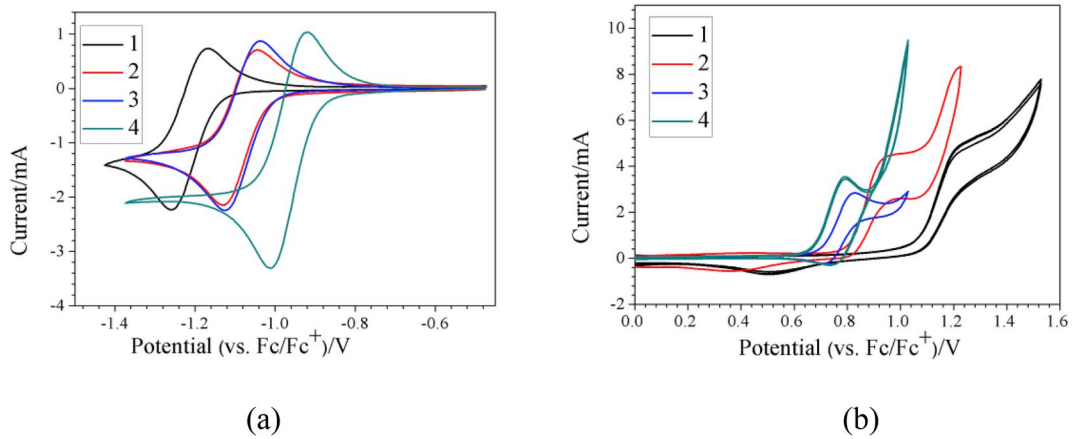

Fig. 3. Cyclic voltammograms for compounds **1**–**4** carried out in 1 M Bu_4NPF_6/CH_2Cl_2 electrolyte in (a) cathodic range; (b) anodic range. Scan speed: 50 mV s^{-1}, sample concentration: 2 mmol dm^{-3}.

electronic state is insignificant, which is a well known phenomenon for numerous rigid BODIPY derivatives [20–23]. At the same time, the Stokes shifts calculated as the difference between the energies of the vertical $S_0 \rightarrow S_1$ and $S_1 \rightarrow S_0$ transitions are significantly overestimated relative to the experimental values. This is because of the energies of the $S_0 \rightarrow S_1$ transitions are considerably overestimated relative to the experimental data, while the energies of the $S_1 \rightarrow S_0$ transitions are oppositely slightly underestimated. This limitation of the TD DFT approximation in respect to BODIPY-core derivatives is well known in the literature. Particularly, Valiev et al. have shown [52,53] that the low-lying S_1, T_1 and T_2 states of the related BODIPY-core systems contain a substantial contribution of double excitation configurations. Multireference methods (like XMCQDPT2 [52]) therefor give the better quantitative agreement between the experimental and theoretical electronic spectra, but at the same time such multireference approaches are computationally much more expensive. Despite this limitation of the TD DFT approach it demonstrates a good linear correlation with experiment and thus can be used to predict the nature of excited states and energies if the latter are corrected empirically [54].

Considering the low-lying positions of the T_1 state for all studied compounds **1**–**4** one can confirm the possible ability of these compounds to exhibit the triplet-triplet annihilation phenomenon [55] observed for some related BODIPY-core derivatives. Extremely small T_1 energies (around 1 eV) make these compounds promising for the singlet oxygen sensitization by energy transfer to oxygen from the triplet exited state of the photosensitizer molecule (BODIPY derivative in our case) [25, 56–59].

4.4. OLED characterization

Accounting for the suppressed aggregation of the studied dyes in the solid state and the acceptable Stokes shifts that prevent light reabsorption and fluorescence self-quenching these materials have been chosen as emissive layers for the fabrication of organic light-emitting devices. Accounting for the PLQY values in a solid film (**1**–5%, **2**–7%, **3**–9%, **4** - 2%) and position of the LUMO and HOMO levels we have fabricated OLEDs based on compounds **2** (devices A, C) and **3** (devices B, D). At the same time, compounds **1** and **4** do not demonstrate a stable electroluminescence within OLED devices. At first, we have tested compounds **2** and **3** as fluorescence emitters in undoped OLEDs (devices A and B). These OLEDs have been than optimized by using CBP as the host material that is suitable for exciton confinement with BODIPY guests 2 and 3 (devices C and D, respectively).

All fabricated OLEDs are characterized by narrow electroluminescence (EL) spectra that is very useful for many applications (like sensitive sensors and co-emitters in multilayered OLEDs). The devices A and C are characterized by pure red emission with EL maximum at 655 nm and full width at half maximum (FWHM) equal to only 45 nm, while devices B and D sustain deeper red emission (EL maximum at 695 nm) and slightly broader EL spectra (FWHM about 60 nm). The EL spectra are stable at different applied voltages (Fig. S5). Comparing the photoluminescence spectra of compounds **2** and **3** in the solid state (Fig. 5) with the corresponding EL spectra of OLEDs, we can see that the latter are even narrower than the PL curves. Most likely this is due to the enhanced molecular rigidity of compounds **2** and **3** within the thin thermovacuum deposited layers in device A that suppresses the fluorescence vibronic progression, well observed in the PL spectra of solution-processed thin solid films (blue lines in Fig. 5) and in the

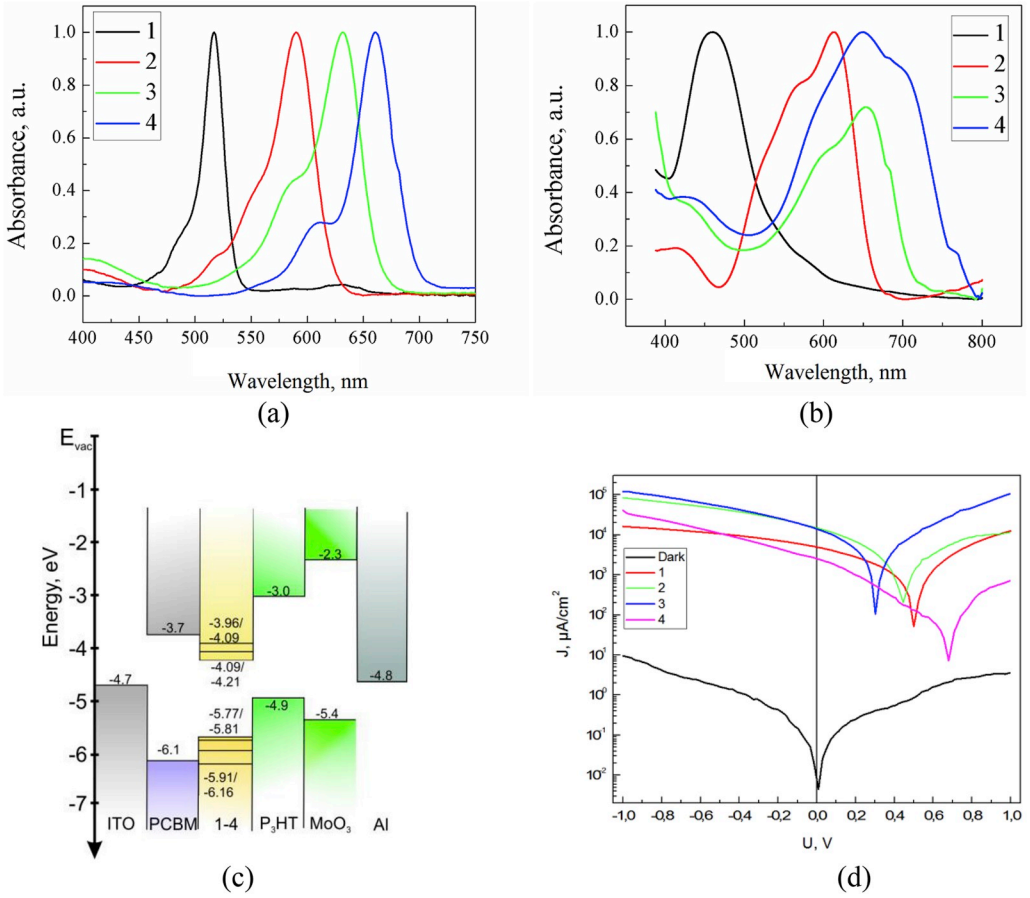

Fig. 4. The absorption spectra of compounds measured in DCM (a) and in the solid film (b). Schematic energy diagram of fabricated OPV cells (c). Short circuit current density (J_{sc}) *vs.* open circuit voltage (V_{oc}) dependences for the fabricated OPV cells (d).

Table 2
Average values of photovoltaic parameters and standard deviations estimated for the 3 fabricated bulk heterojunction in parallel based on every BODIPY derivative **1**–**4**.

Compound	1	2	3	4
Isc, μA	−29.713 ± 0.079	−87.203 ± 0.088	−83.752 ± 0.073	−1.501 ± 0.065
V_{oc}, mV	500 ± 8	449 ± 8	305 ± 5	660 ± 7
I_{max}, μA	−13.834 ± 0.035	−41.440 ± 0.040	−37.782 ± 0.038	−0.780 ± 0.021
V_{max}, mV	250 ± 4	197 ± 3	155 ± 9	155 ± 8
FF	0.230 ± 0.004	0.208 ± 0.005	0.230 ± 0.009	0.122 ± 0.005
η, %	0.60 ± 0.03	1.36 ± 0.04	1.00 ± 0.07	0.20 ± 0.04

luminescence spectra measured in diluted DCM solutions.

The additional PL band around 525 nm (Fig. 5c and d) most likely corresponds to emission from aggregates of the studied dyes that are formed in the solid film. In the absorption spectra measured in the solid film (Fig. 4b), a band around 450 nm is observed for compounds **2** and **3** that is most probably corresponding to these aggregates. At the same time in the EL spectra of doped and undoped devices the emission band around 450 nm is clearly absent, meaning that aggregates are not formed in the mixed host-guest film neither are dimer-localized excitons formed upon applied bias. It seems that in the neat solid state film the BODIPY dyes are partially aggregated (only partially, because the main band is still not-shifted and most intensive) and these aggregates demonstrate a blue-shifted absorption and emission (H-type aggregates). Also, it is clear that the less branched compound **3** (Fig. 1) demonstrates the clearer visible PL band at 525 nm while the more

Table 3
Photophysical constants for compounds **1**–**4** calculated at the TD DFT level of theory in comparison with experimental data.

	λ_{abs}, nm (ε, $M^{-1}cm^{-1}$)[a]	λ_{em}, nm (Φ_f)[a]	λ_{abs}(vert.), nm	λ_{em} (vert.), nm	$E_{vert}(T_1)$, nm	Δν, nm
1	519 (122000)	535 (0.98)	461 [0.832]	553 [0.829]	775	92 (16)[a]
2	586 (95000)	614 (0.73)	461 [0.882]	600 [0.946]	964	92 (28)[a]
3	633 (93000)	658 (0.69)	461 [1.080]	692 [1.220]	1090	104 (25)[a]
4	658 (126000)	683 (0.74)	461 [1.020]	681 [1.120]	1158	104 (25)[a]

Oscillator strengths for corresponding vertical electronic transitions are presented in brackets.
Δν corresponds to the Stokes shift value.
[a] Measured experimentally in DCM solutions [20–23].

branched compound **2** demonstrates only a weak PL shoulder at 525 nm.

The lighting characteristics of the fabricated devices are presented in Fig. 6 and also are summarized in Table 4. One can conclude from these data that the designed OLEDs demonstrate stable luminance performance in a wide range of current density regimes implying that the used BODIPY derivatives are stable with respect to the applied bias. Undoped devices A and B are characterized by a high turn-on voltage, however, the optimized (doped) devices B and D expectedly demonstrate a decrease of turn on voltage (Table 4). Additionally, the usage of CBP as a host increases the external quantum efficiency and brightness of the doped devices C and D relative to the undoped ones (Fig. 6, Table 4). The

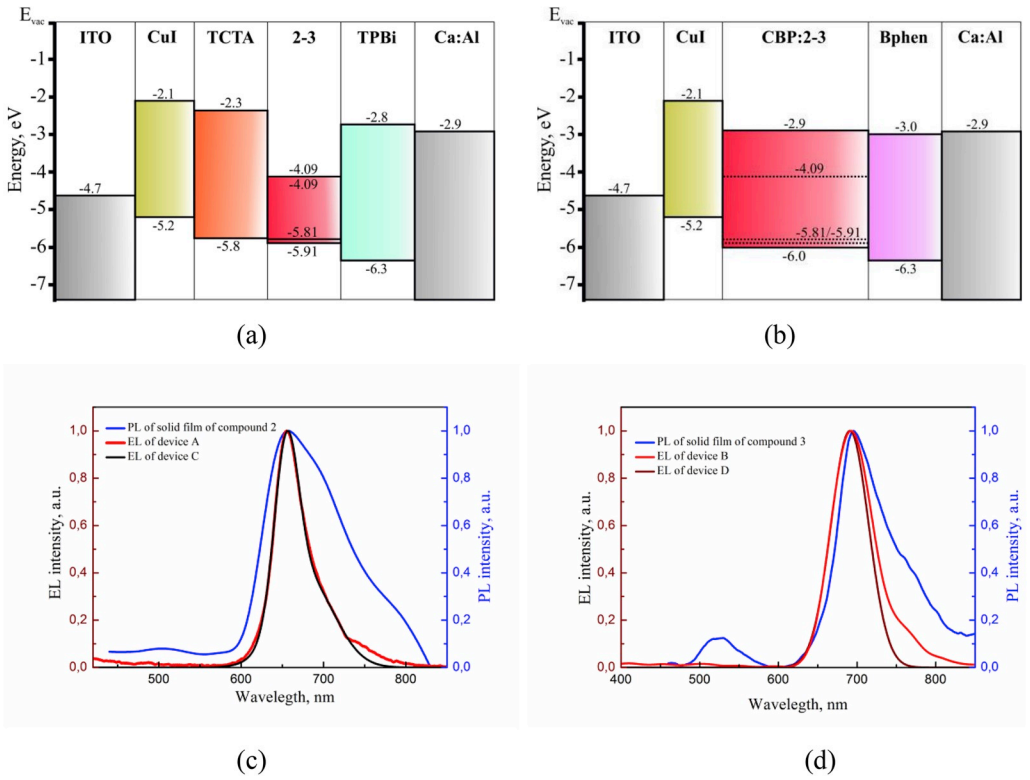

Fig. 5. Energy diagrams of fabricated OLEDs A, B (a) and C, D (b). Thin solid films PL spectra of the compounds **2 (c)** and **3 (d)** compared with the EL spectra of devices A-D.

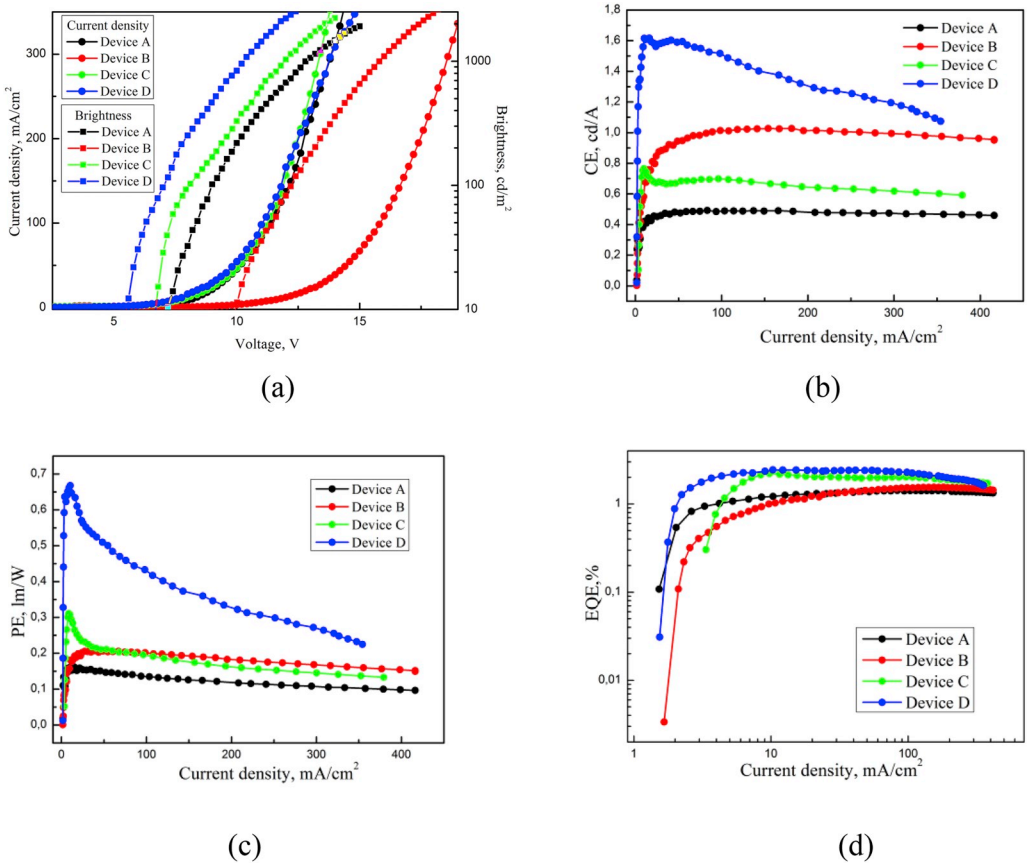

Fig. 6. The current density/luminance vs. voltage (a), current efficiency (CE) *vs.* current density (b), photoefficiency (PE) *vs.* current density (c) and external quantum efficiency (EQE) *vs.* current density (d) characteristics of OLEDs A-D.

Table 4
Lightning characteristics of OLEDs A-D.

Device	V_{on}[a] at 10 Cd m^{-2}, V	Brightness at 15 V/max., Cd/m^2	Current efficiency, Cd/A	EQE,[a] %	CIE 1931, (x, y)
			at 100/1000 Cd m^{-2}		
A	6.6	1900/1900	0.45/0.47	1.3/1.3	(0.55,0.28)
B	9.0	700/3900	0.7/1.0	1.0/1.5	(0.42,0.28)
C	6.2	2200/2200	0.7/0.6	2.0/1.9	(0.55, 0.28)
D	5.2	3800/3800	1.49/1.55	2.2/2.3	(0.42,0.28)

[a] EQE – external quantum efficiency, %; V_{on} – turn on voltage of OLED.

EQE roll-off for all these devices is insignificant, probably because of the balanced charge capture ability in the emissive layer. However, the main advantage of the fabricated devices refers to the narrow electroluminescence spectra and pure red colour CIE coordinates, which is useful for RGB scheme applications and sensitive optical sensors.

5. Conclusions

In the present paper we have studied a series of BODIPY dyes functionalized by different substituents in the α/β-positions with condensed pyridine-2(1*H*)-one groups as light harvesting and emissive materials for bulk heterojunction solar cells and organic light-emitting diodes, respectively. The fabricated photovoltaic cells demonstrate a clear dependence between the energies of the HOMO/LUMO levels of the BODIPY light absorbers and the overall device performance due to the increase of the energy barriers at the interface between the dye and the electron transporting PCBM material. A similar "orbital" effect was also observed for the prepared OLEDs - the very low energy of the LUMO level of the BODIPY derivatives causes a complicated electron injection into the emissive layer. Despite such limitations, the best fabricated photovoltaic device based on the BODIPY dye **2** demonstrates a performance of about 1.36% which is among the best results for related bulk heterojunction solar cells based on various BODIPY derivatives.

Doped and undoped deep red OLEDs with narrow electroluminescence spectra (full width at half maximum up to 45 nm) were fabricated in this work. The best doped device demonstrates a maximum brightness of 3900 cd m^{-2} and an external quantum efficiency of 2.3%, being also at the same level as the previously published fluorescence analogues. Theoretical calculations of the first triplet excited state energies predict a low-lying position of this state (around 1 eV) that could be useful for inducing singlet oxygen sensitization and triplet-triplet annihilation processes.

Declaration of competing interest

The authors declare that they have no known competing financial interests or personal relationships that could have appeared to influence the work reported in this paper.

CRediT authorship contribution statement

K. Ivaniuk: Investigation, Formal analysis. **A. Pidluzhna:** Investigation, Formal analysis, Visualization. **P. Stakhira:** Conceptualization, Supervision. **G.V. Baryshnikov:** Conceptualization, Writing - original draft, Software, Project administration. **Y.P. Kovtun:** Resources, Investigation. **Z. Hotra:** Project administration, Writing - review & editing, Supervision. **B.F. Minaev:** Project administration, Writing - review & editing, Supervision. **H. Ågren:** Project administration, Writing - review & editing, Supervision, Funding acquisition.

Acknowledgements

This work was supported by the Ministry of Education and Science of Ukraine (projects no. 0117U003908 and 0119U100259). G.B. and H.Å. also thankful for the financial support by the Olle Engkvist Byggmästare Foundation (contract No. 189-0223). This project has received funding from the European Union's Horizon 2020 research and innovation programme under the Marie Skłodowska-Curie grant agreement No 823720. The quantum-chemical calculations were performed with computational resources provided by the High Performance Computing Center North (HPC2N) in Umeå, Sweden, through the project "Multi-physics Modeling of Molecular Materials" SNIC 2018-2-38.

Appendix A. Supplementary data

Supplementary data to this article can be found online at https://doi.org/10.1016/j.dyepig.2019.108123.

References

[1] Tessler N, Medvedev V, Kazes M, Kan S, Banin U. Efficient near-infrared polymer nanocrystal light-emitting diodes. Science 2002;295:1506. https://doi.org/10.1126/science.1068153.
[2] Qian G, Zhong Z, Luo M, Yu D, Zhang Z, Wang ZY, Ma D. Simple and efficient near-infrared organic chromophores for light-emitting diodes with single electroluminescent emission above 1000 nm. Adv Mater 2009;21(1):111–6. https://doi.org/10.1002/adma.200801918.
[3] Escobedo JO, Rusin O, Lim S, Strongin RM. NIR dyes for bioimaging applications. Curr Chem Biol 2010;14(1):64–70. https://doi.org/10.1016/j.cbpa.2009.10.022.
[4] Chapran M, Angioni E, Findlay NJ, Breig B, Cherpak V, Stakhira P, Tuttle T, Volyniuk D, Grazulevicius JV, Nastishin YuA, Lavrentovich OD, Skabara PJ. An ambipolar BODIPY derivative for a white exciplex OLED and cholesteric liquid crystal laser toward multifunctional devices. ACS Appl Mater Interfaces 2017;9(5):4750–7. https://doi.org/10.1021/acsami.6b13689.
[5] Rousseau T, Cravino A, Bura T, Ulrich G, Ziessel R, Roncali J. BODIPY derivatives as donor materials for bulk heterojunction solar cells. Chem Commun 2009;13:1673–5. https://doi.org/10.1039/B822770E.
[6] Kolemen S, Cakmak Y, Erten-Ela S, Altay Y, Brendel J, Thelakkat M, Akkaya EU. Solid-state dye-sensitized solar cells using red and near-IR absorbing BODIPY sensitizers. Org Lett 2010;12(17):3812–5. https://doi.org/10.1021/ol1014762.
[7] Loudet A, Burgess K. BODIPY dyes and their derivatives: syntheses and spectroscopic properties. Chem Rev 2007;107:4891–932. https://doi.org/10.1021/cr078381n.
[8] Ziessel R, Ulrich G, Harriman A. The chemistry of fluorescent BODIPY dyes: versatility unsurpassed. Angew Chem 2008;47:1184–201. https://doi.org/10.1002/anie.200702070.
[9] Benstead M, Mehl GH, Boyle RW. 4,4'-Difluoro-4-bora-3a,4a-diaza-s-indacenes (BODIPYs) as components of novel light active materials. Tetrahedron 2011;67:3573–601. https://doi.org/10.1016/j.tet.2011.03.028.
[10] Boens N, Leen V, Dehaen W. Fluorescent indicators based on BODIPY. Chem Soc Rev 2012;41:1130–72. https://doi.org/10.1039/C1CS15132K.
[11] Umezawa K, Citterio D, Suzuki K. New trends in near-infrared fluorophores for bioimaging. Anal Sci 2014;14:327–49. https://doi.org/10.2116/analsci.30.327.
[12] Lu H, Mack J, Yanga Y, Shen Z. Structural modification strategies for the rational design of red/NIR region BODIPYs. Chem Soc Rev 2014;43:4778–823. https://doi.org/10.1039/C4CS00030G.
[13] Nia Y, Wu J. Far-red and near infrared BODIPY dyes: synthesis and applications for fluorescent pH probes and bio-imaging. Org Biomol Chem 2014;12:3774–91. https://doi.org/10.1039/C3OB42554A.
[14] Sing SP, Gayathri T. Evolution of BODIPY dyes as potential sensitizers for dyesensitized solar cells. Eur J Org Chem 2014;22:4689–707. https://doi.org/10.1002/ejoc.201400093.
[15] Boens N, Verbelen B, Dehaen W. Postfunctionalization of the BODIPY core: synthesis and spectroscopy. Eur J Org Chem 2015;30:6577–95. https://doi.org/10.1002/ejoc.201500682.
[16] Bañuelos J. BODIPY dye, the most versatile fluorophore ever? Chem Rec 2016;16:335–48. https://doi.org/10.1002/tcr.201500238.
[17] Zatsikha YV, Kovtun YP. The main strategies of design and applications of BODIPYs. In: Kadish KM, Smith KM, Guilard R, editors. The handbook of pophyrin science, vol. 36. Singapore: World Scientific Publishing; 2016. p. 151–257. https://doi.org/10.1142/9789813149564_0002.
[18] Clarke RG, Hall MJ. Recent developments in the synthesis of the BODIPY dyes. Adv Heterocycl Chem 2019;128:181–261. https://doi.org/10.1016/bs.aihch.2018.12.001.
[19] Kim NH, Kim D. Blue-emitting BODIPY dyes. In: Sola- Llano R, Bañuelos-Prieto J, editors. BODIPY dyes - a privilege molecular scaffold with tunable properties. IntechOpen; 2019. p. 297–348. https://doi.org/10.5772/intechopen.75220.
[20] Shandura MP, Yakubovskyi VP, Kovtun YP. (4,4-Difluoro-4-bora-3a,4a,-diaza-s-indacen-3-yl)acetaldehyde: synthesis and chemical properties. J Heterocycl Chem 2009;46(6):1386–91. https://doi.org/10.1002/jhet.263.

[21] Zatsikha YV, Yakubovskyi VP, Shandura MP, Dubey IY, Kovtun YP. An efficient method of chemical modification of BODIPY core. Tetrahedron 2013;69(10): 2233–8. https://doi.org/10.1016/j.tet.2013.01.050.
[22] Shandura MP, Yakubovskyi VP, Gerasov AO, Kachkovsky OD, Poronik YM, Kovtun YP. α-Polymethine-substituted boron dipyrromethenes – BODIPY-based NIR cyanine-like dyes. Eur J Org Chem 2012;9:1825–34. https://doi.org/10.1002/ejoc.201101674.
[23] Zatsikha YV, Yakubovskyi VP, Shandura MP, Kovtun YP. Functionalized bispyridoneannelated BODIPY – bright long-wavelength fluorophores. Dyes Pigments 2015;114:215–21. https://doi.org/10.1016/j.dyepig.2014.11.016.
[24] Nakashima M, Iizuka K, Karasawa M, Ishii K, Kubo Y. Selenium-containing BODIPY dyes as photosensitizers for triplet–triplet annihilation upconversion. J Mater Chem C 2018;6:6208–15. https://doi.org/10.1039/C8TC00944A.
[25] Zhao J, Xu K, Yang W, Wang Z, Zhong F. The triplet excited state of BODIPY: formation, modulation and application. Chem Soc Rev 2015;44:8904–39. https://doi.org/10.1039/C5CS00364D.
[26] Zhou Q, Zhou M, Wei Y, Zhou X, Liu S, Zhang S, Zhang B. Solvent effect on triplet-triplet annihilation upconversion of diiodo-BODIPY and perylene. Phys Chem Chem Phys 2017;19:1516–25. https://doi.org/10.1039/C6CP06897A.
[27] Merkushev DA, Usoltsev SD, Marfin YS, Pushkarev AP, Volyniuk D, Grazulevicius JV, et al. BODIPY associates in organic matrices: spectral properties, photostability and evaluation as OLED emitters. Mater Chem Phys 2017;187: 104–11. https://doi.org/10.1016/j.matchemphys.2016.11.053.
[28] Zampetti A, Minotto A, Squeo BM, Gregoriou VG, Allard S, Scherf U, Chochos CL, Cacialli F. Highly efficient solid-state near-infrared organic light-emitting diodes incorporating A-D-A dyes based on α,β-unsubstituted "BODIPY" moieties. Sci Rep 2017;7:1611. https://doi.org/10.1038/s41598-017-01785-2.
[29] Cardona CM, Li W, Kaifer AE, Stockdale D, Bazan GC. Electrochemical considerations for determining absolute frontier orbital energy levels of conjugated polymers for solar cell Applications. Adv Mater 2011;23:2367–71. https://doi.org/10.1002/adma.201004554.
[30] Hotra Z, Stakhira P, Cherpak V, Volynyuk D, Voznyak L, Gorbulyk V, Tsizh B. Effect of thickness of a CuI hole injection layer on the properties of organic light emitting diodes. Photon Lett Pol 2012;4(1):35–7. https://doi.org/10.4302/plp.2012.1.13.
[31] Huang J, Yang X, Li X, Chen P, Tang R, Li F, Lu P, Ma Y, Wang L, Qin J, Lia Q, Li Z. Bipolar AIE-active luminogens comprised of an oxadiazole core and terminal TPE moieties as a new type of host for doped electroluminescence. Chem Commun 2012;44:9586–8. https://doi.org/10.1039/C2CC34966C.
[32] Ivaniuk Kh, Cherpak V, Stakhira P, Hotra Z, Minaev B, Baryshnikov G, Stromylo E, Volyniuk D, Grazulevicius JV, Lazauskas A, Tamulevicius S, Witulski B, Light ME, Gawrys P, Whitby RJ, Wiosna-Salyga G, Luszczynska B. Highly luminous sky-blue organic light-emitting diodes based on the bis [(1, 2)(5, 6)] indoloanthracene emissive layer. J Chem Phys C 2016;11:6206–17. https://doi.org/10.1021/acs.jpcc.6b00696.
[33] Perumal A, Faber H, Yaacobi-Gross N, Pattanasattayavong P, Burgess C, Jha S, McLachlan MA, Stavrinou PN, Anthopoulos TD, Bradley DDC. High-efficiency, solution-processed, multilayer phosphorescent organic light-emitting diodes with a copper thiocyanate hole-injection/hole-transport layer. Adv Mater 2015;7:93–100. https://doi.org/10.1002/adma.201403914.
[34] Yang C, Lee JH, Chen C-T. Synthesis, photoluminescence, and electroluminescence characterization of double tetraphenylethene-tethered BODIPY luminogens. J Chin Chem Soc 2019;1–12. https://doi.org/10.1002/jccs.201900163.
[35] Becke AD. Density-functional thermochemistry. III. The role of exact exchange. J Chem Phys 1993;98:5648–52. https://doi.org/10.1063/1.464913.
[36] Lee C, Yang W, Par RG. Development of the Colle-Salvetti correlation-energy formula into a functional of the electron density. Phys Rev B 1988;37:785–9. https://doi.org/10.1103/PhysRevB.37.785.
[37] Ditchfield R, Hehre WJ, Pople JA. Self-consistent molecular-orbital methods. IX. An extended Gaussian-type basis for molecular-orbital studies of organic molecules. J Chem Phys 1971;54:724–8. https://doi.org/10.1063/1.1674902.
[38] Bauernschmitt R, Ahlrichs R. Treatment of electronic excitations within the adiabatic approximation of time dependent density functional theory. Chem Phys Lett 1996;256:454–64. https://doi.org/10.1016/0009-2614(96)00440-X.
[39] Tomasi J, Mennucci B, Cammi R. Quantum mechanical continuum solvation models. Chem Rev 2005;105(8):2999–3094. https://doi.org/10.1021/cr9904009.
[40] Frisch MJ, Trucks GW, Schlegel HB, Scuseria GE, Robb MA, Cheeseman JR, et al. Gaussian 16, revision A.03. Wallingford CT: Gaussian, Inc.; 2016.
[41] Takimiya K, Osaka I, Nakano M. π-Building blocks for organic electronics: revaluation of "Inductive" and "Resonance" effects of π-electron deficient units. Chem Mater 2013;26:587–93. https://doi.org/10.1021/cm4021063.
[42] Kurowska A, Brzeczek-Szafran A, Zassowski P, Lapkowski M, Domagala W, Wagner P, Wagner K. Mono and di-substituted BODIPY with electron donating carbazole, thiophene, and 3,4-ethylenedioxythiophene units. Electrochim Acta 2018;271:685–98. https://doi.org/10.1016/j.electacta.2018.03.044.
[43] Poe AM, Della Pelle AM, Subrahmanyam AV, White W, Wantz G, Thayumanavan S. Small molecule BODIPY dyes as non-fullerene acceptors in bulk heterojunction organic photovoltaics. Chem Commun 2014;22:2913–5. https://doi.org/10.1039/C3CC49648A.
[44] Lu L, Zheng T, Wu Q, Schneider AM, Zhao D, Yu L. Recent advances in bulk heterojunction polymer solar cells. Chem Rev 2015;115:12666–731. https://doi.org/10.1021/acs.chemrev.5b00098.
[45] Wei H, Scudiero L, Eilers H. Infrared and photoelectron spectroscopy study of vapor phase deposited poly (3-hexylthiophene). Appl Surf Sci 2009;255:8593–7. https://doi.org/10.1016/j.apsusc.2009.06.031.
[46] Rodrigues AM, Castro C, Andreia RS, Farinha F, Oliveira M, Tomé João PC, Machado AV, Raposo M, Hilliou L, Bernardo G. Thermal stability of P3HT and P3HT:PCBM blends in the molten state. Polym Test 2013;32:1192–201. https://doi.org/10.1016/j.polymertesting.2013.07.008.
[47] Kim JY, Lee K, Coates NE, Moses D, Nguyen T-Q, Dante M, Heeger AJ. Efficient tandem polymer solar cells fabricated by all-solution processing. Science 2007;317: 222–5. https://doi.org/10.1126/science.1141711.
[48] Baran D, Tuladhar S, Economopoulos SP, Neophytou M, Savva A, Itskos G, Othonos A, Bradley DDC, Brabeca CJ, Nelson J, Choulis SA. Photovoltaic limitations of BODIPY:fullerene based bulk heterojunction solar cells. Synth Met 2017;226:25–30. https://doi.org/10.1016/j.synthmet.2017.01.006.
[49] Kolemen S, Cakmak Y, Ozdemira T, Erten-Ela S, Buyuktemiz M, Dede Y, Akkaya EU. Design and characterization of BODIPY derivatives for bulk heterojunction solar cells. Tetrahedron 2014;70:6229–34. https://doi.org/10.1016/j.tet.2014.03.049.
[50] Tokoro Y, Nagai A, Chujo Y. Nanoparticles via H-aggregation of amphiphilic BODIPY dyes. Tetrahedron Lett 2010;51:3451–4. https://doi.org/10.1016/j.tetlet.2010.04.120.
[51] Mikhalyov I, Gretskaya N, Bergström F, Johansson LB-A. Electronic ground and excited state properties of dipyrrometheneboron difluoride (BODIPY): dimers with application to biosciences. Phys Chem Chem Phys 2002;4:5663–70. https://doi.org/10.1039/B206357N.
[52] Valiev RR, Telminov EN, Solodov TA, Ponyavina EN, Gadirov RM, Mayer GV, Kopylova TN. Lasing of pyrromethene 567 in solid matrices. Chem Phys Lett 2013; 588:184–7. https://doi.org/10.1016/j.cplett.2013.10.019.
[53] Valiev RR, Sinelnikov AN, Aksenov YV, Kuznetsov RT, Berezin MB, Semeikin AS, Cherepanov VN. The computational and experimental investigations of photophysical and spectroscopic properties of BF_2 dipyrromethene complexes. Spectrochim Acta Part A Mol Biomol Spectrosc 2014;117:323–9. https://doi.org/10.1016/j.saa.2013.08.042.
[54] Mohammad R, Brown M, Brown A. Why Do TD-DFT excitation energies of bodipy/aza-bodipy families largely deviate from experiment? Answers from electron correlated and multireference methods. J Chem Theory Comput 2015;11(6): 2619–32. https://doi.org/10.1021/ct500775r.
[55] Minaev BF. Theoretical model of triplet-triplet annihilation. Sov Phys J 1978;21 (9):1120–4. https://doi.org/10.1007/BF00894558.
[56] Semyachkina-Glushkovskaya OV, Sokolovski SG, Goltsov A, Gekaluyk AS, Saranceva EI, Bragina OA, Tuchine VV, Rafailov EU. Laser-induced generation of singlet oxygen and its role in the cerebrovascular physiology. Prog Quantum Electron 2017;55:112–28. https://doi.org/10.1016/j.pquantelec.2017.05.001.
[57] Minaev B. Photochemistry and spectroscopy of singlet oxygen in solvents. recent advances which support the old theory. Chem Chem Technol 2016;10(4s):519–30. https://doi.org/10.23939/chcht10.04si.519.
[58] Minaev BF, Minaeva VA, Evtuhov YV. Quantum-chemical study of the singlet oxygen emission. Int J Quantum Chem 2009;109:500–15. https://doi.org/10.1002/qua.21783.
[59] Minaev BF, Minaeva VA. MCSCF response calculations of the excited states properties of the O_2 molecule and a part of its spectrum. Phys Chem Chem Phys 2002;3:720–9. https://doi.org/10.1039/b006712l.